

Overview of Magnetic Resonance Fingerprinting

Simone Coppo¹; Bhairav B. Mehta¹; Debra McGivney¹; Dan Ma¹; Yong Chen¹; Yun Jiang²; Jesse Hamilton²; Shivani Pahwa¹; Chaitra Badve¹; Nicole Seiberlich¹; Mark Griswold^{1,2}; Vikas Gulani¹

Departments of Radiology (1) and Biomedical Engineering (2), Case Western Reserve University, University Hospitals Case Medical Center, Cleveland, OH, USA

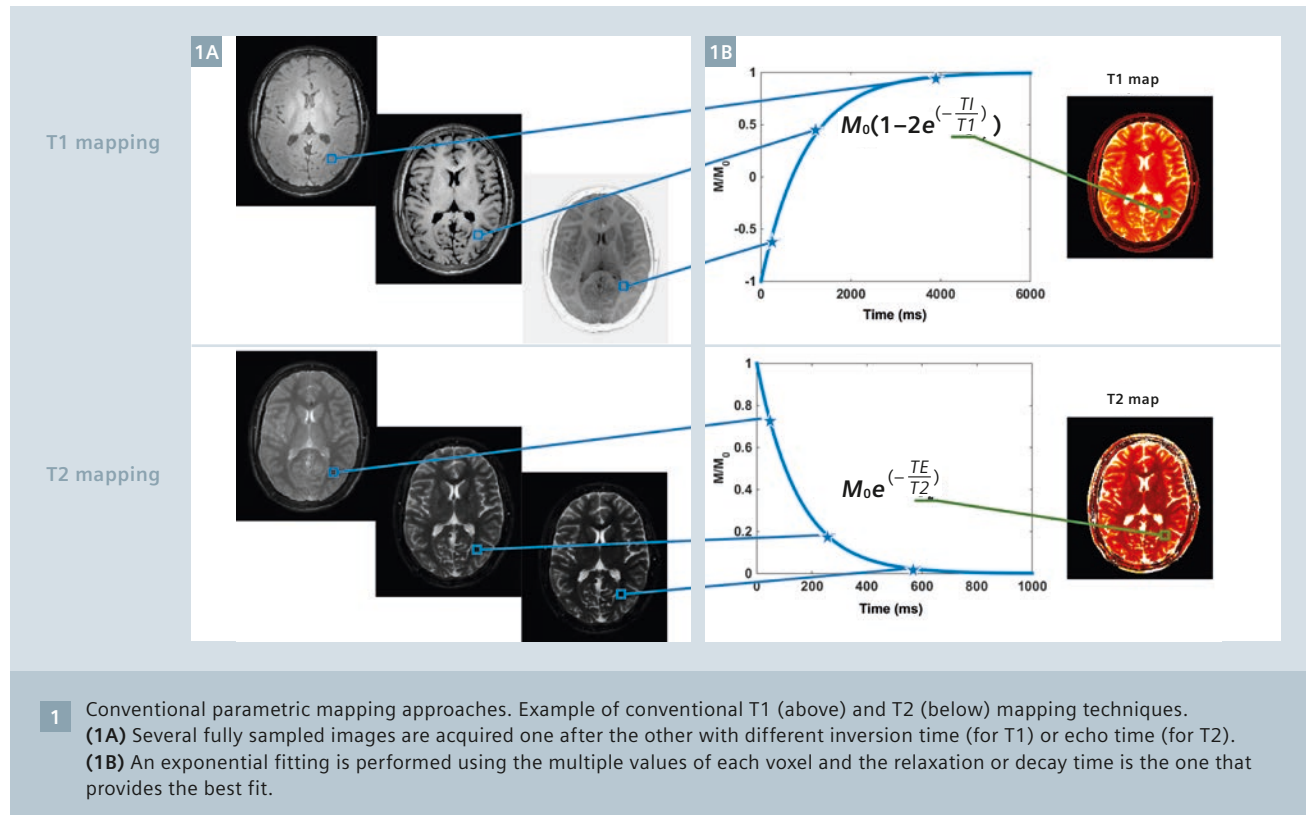
Introduction

Magnetic Resonance Imaging (MRI) is a powerful diagnostic, prognostic and therapy assessment tool due to its versatile nature as compared to other imaging modalities, as MRI allows the user to probe and measure various kinds of information (T1, T2, B₀, diffusion, perfusion, etc.). However, MRI has the drawback of being slow compared to other diagnostic tools, and is generally qualitative, where the contrast between tissues, rather than absolute measurements from single tissues, is the primary means of information that is used to characterize an underlying

pathology. While this information has proven extremely valuable for diagnosis, prognosis, and therapeutic assessment, the lack of quantification limits objective evaluation, leads to a variability in interpretation, and potentially limits the utility of the technology in some clinical scenarios.

To overcome this limitation, significant effort has been put into developing quantitative approaches that can measure tissue proprieties such as T1 and T2 relaxation times. Quantifying tissue proprieties allows physicians to better distinguish between healthy and pathological

tissue [1] in an absolute sense, makes it easier to objectively compare different exams in follow-up studies [2], and could be more representative of the underlying changes at the cellular level [3, 4] than standard weighted imaging. Quantitative imaging is crucial in the assessment of disease settings presenting subtle features such as cardiac diffuse fibrosis [5], iron [6] or fat deposition in the liver [7]. Additionally, there are various clinical settings in which multiple features such as T1, T2, diffusion, etc. add up synergistically to drastically improve the information for diagnosis, prognosis and/or therapeutic assessment.



While quantitative imaging has been a long-standing goal of the MR community, a drawback encountered in early conventional quantitative imaging was the reduced time efficiency compared to qualitative imaging. Early conventional approaches for T1 and T2 mapping involved measuring one parameter at a time. These techniques relied on the acquisitions of several images, each with one specific acquisition parameter that varies for each image while the others were kept constant (Fig. 1A). The obtained images were subsequently fitted with a mathematical model to estimate the one parameter of interest, for example the relaxation time (T1) [8] or the time of signal decay (T2) [9] (Fig. 1B). This process had to be repeated for each parameter of interest. The need for keeping all except one sequence parameter and signal state constant and the limitation of assessing one parameter at a time made these approaches extremely time-inefficient because of the prolonged scan time and thus not suitable for a clinical environment where interscan motion can render such approaches infeasible. In recent times, several approaches have been proposed to shorten the acquisition time [10–13] or to provide combined T1 and T2 measurements [14–18] within a single acquisition. However, major barriers remain to clinical adoption, most notably a simultaneous need for rapid and accurate quantification.

To overcome the common drawbacks of quantitative imaging, Magnetic Resonance Fingerprinting (MRF)¹ [19–21] has been recently developed. This technique aims at providing simultaneous measurements of multiple parameters such as T1, T2, relative spin density, B_0 inhomogeneity (off-resonance frequency), etc., using a single, time-efficient acquisition. MRF completely changes the way quantitative MRI is performed with

an entirely different approach from that of conventional techniques. Instead of performing an acquisition with all but one sequence parameter constant, MRF relies on deliberately varying acquisition parameters in a pseudorandom fashion such that each tissue generates a unique signal evolution. It is possible to simulate signal evolutions from first principles using different physical models for a wide variety of tissue parameter combinations, which are collected together in a database called dictionary. After the acquisition, a pattern recognition algorithm is used to find the dictionary entry that best represents the acquired signal evolution of each voxel. The parameters that were used to simulate the resulting best match are then assigned to the voxel. This process is analogous to the fingerprinting identification process used by forensic experts to identify persons of interest. The acquired signal evolution is unique for each tissue and can be seen as the collected fingerprint that has to be identified. The dictionary is equivalent to the database where all the known fingerprints are stored, together with all the information relative to each person. In the forensic case, each fingerprint points to the feature identification of the associated person such as name, height, weight, eye color, date of birth, etc. Similarly, in the case of MRF, each fingerprint in the dictionary points to the MR related identification features of the associated tissue such as T1, T2, relative spin density, B_0 , diffusion, etc. After the acquisition, the fingerprint contained in a voxel is compared with all the entries in the dictionary. The dictionary entry that best matches the acquired fingerprint is considered a positive match, meaning that the tissue represented in the voxel has been identified. All the known parameters relative to that fingerprint can then be retrieved from the dictionary and assigned to the voxel. The uniqueness of the different signal components and the accuracy with which the dictionary is simulated are two crucial components for the correct estimation of the tissue parameters.

This paper attempts to describe the basic concepts of MRF and illustrate some clinical applications.

Acquisition sequence

Standard quantitative MR imaging approaches require several acquisitions, each one of which constantly repeats the same acquisition pattern, such as radiofrequency excitation angle (flip angle, FA), repetition time (TR) and gradient patterns, until all required data in the Fourier domain (also called k -space) are obtained. Each image is then reconstructed using the Fourier transform and a nonlinear fitting process is applied to each voxel. With MRF, instead, the flip angle, the TR and the trajectory (Fig. 2A, B) vary in a pseudorandom fashion throughout the acquisition; when implemented properly, this generates uncorrelated signals for each tissue, providing the unique fingerprints that are used to recognize the tissue. The initial implementation of MRF [19] was based on a balanced steady-state free-precession (bSSFP or TrueFISP) sequence because of its sensitivity to T1, T2 and off-resonance frequency, and because the steady-state signal generated by this sequence has been thoroughly studied [22]. The FA (Fig. 2A) varies in a sinusoidal fashion to smoothly vary the transient state of the magnetization, ranging from 0° to 60° and from 0° to 30° alternatively, with a period of 250 time points, or images. On top of this signal, a random variation is added to induce differences in the time evolutions from tissues with similar parameters. After each half period (250 images), 50 flip angles are set to 0° to allow for signal recovery. The TR variations, instead, are based on Perlin noise [23] which ranges from 9.34 ms to 12 ms. These are only examples of how the parameters can be randomly varied. Other random patterns have been tested [19, 24] showing that MRF is not limited to one specified set of parameters.

An inversion recovery pulse is played out at the beginning of the acquisition sequence to enhance T1 differences between tissues (Fig. 2B). For each TR, a heavily undersampled

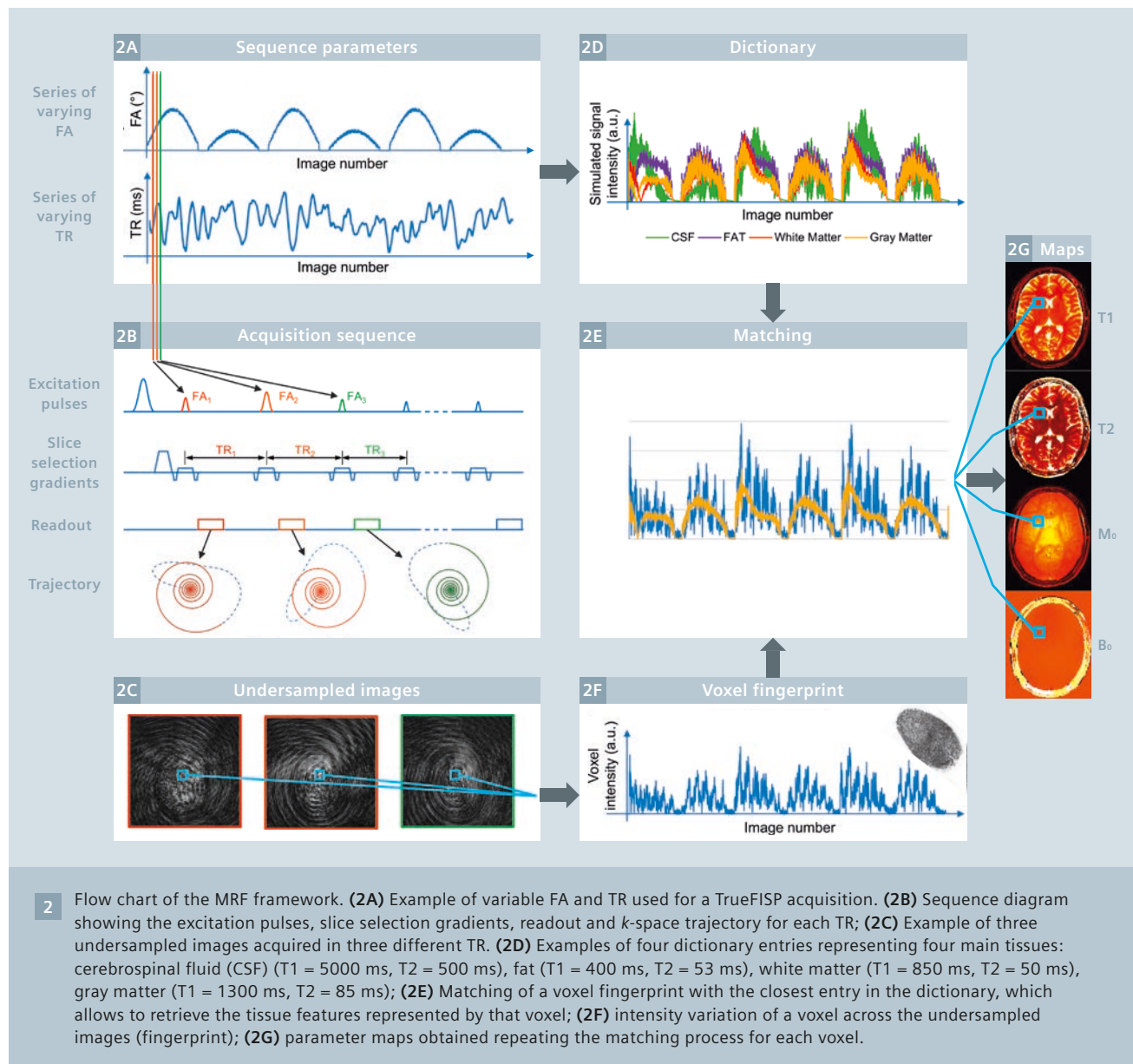
¹ The product is still under development and not commercially available yet. Its future availability cannot be ensured. As this is a research topic in predevelopment, all results shown are preliminary in nature and do not allow for generalizations or conclusions to be drawn. Product realization and features therein cannot be assured as the product may undergo further design iterations.

image is reconstructed (Fig. 2C). It can be noticed how the base image series are not useful by themselves, but each voxel contains a signature fingerprint that will be used later on for the matching (identification). The total number of images acquired (also referred to as 'time points') can vary from acquisition to acquisition, ranging from 1000 [19] to 2500 [21] as function of the image resolution, the undersampling ratio, the matching approach used, etc. In most cases, we have used a variable-density spiral trajectory [25] designed to have a minimum time gradient and zero moment compensation for the acquisition. For example, we

have successfully used a trajectory for a 128×128 matrix size that requires one interleaf to fully sample the center of k -space and 48 interleaves to fully sample the outer region of k -space. In the case of a 256×256 matrix, a trajectory requiring 24 interleaves to fully sample the inner region and 48 interleaves to fully sample the outer region can be used instead. Within each TR, one interleaf is acquired and used to reconstruct an image (or time point). The interleaf in the following TR is then rotated by 7.5° ($\approx 2\pi/48$) compared to the previous one.

The MRF framework is not only limited to a TrueFISP-based acquisi-

tion, but can be virtually applied to any kind of sequence. As an example, the MRF framework has been applied to a steady-state precession sequence (FISP) [20] to avoid the banding artifacts that can appear in wide field-of-view scans or in a high-field-strength scanner. The FISP sequence is still sensitive to T1 and T2 components but is less sensitive to off-resonance frequency. This is caused by the unbalanced gradient within every TR which results in the signal to be the sum of the spins within a voxel, making the sequence immune to banding artifacts. The unbalanced gradient, though, leads the FISP sequence to have a shorter transient state com-



pared to the TrueFISP. For this reason, the pseudorandom FA variation needs to be generated slightly differently than in the case of the TrueFISP sequence, in order to keep incoherence between the signal and under-sampling artifacts and to be able to identify the underlying fingerprint. The FA variation is thus generated based on sinusoidal variation in which the maximum reached FA for each half period randomly changes, ranging from 5° to 90°. The TR variation is always based on a Perlin noise pattern which ranges from 11.5 ms to 14 ms.

Dictionary generation

The dictionary can be seen as the heart of the MRF framework; it is the database that contains all physiologically possible signal evolutions that may be observed from the acquisition and that makes it possible to recognize the tissue within each voxel. MRF, like the forensic fingerprinting identification process, is effective only when a database large enough to contain all the potential candidates is available. In MRF, the dictionary is generated on a computer using algorithms that simulate the spin behavior during the acquisition and thus predict the realistic signal evolution. In case of a TrueFISP-based acquisition, the Bloch equations [26] are used to simulate the various effects of the acquisition sequence on the spins, given a set of tissue parameters of interest (Fig. 2D). The information that can be retrieved with MRF is thus related to how and what physical effects are simulated. In the initial stages of development, MRF includes the simulation of T1, T2 and off-resonance, but more tissue features can be simulated and extracted, such as partial volume [19], diffusion [27] and perfusion [28].

A critical aspect of the dictionary is its size: to ensure the identification of any possible tissue parameter present in the acquisition, a wide combination of T1, T2 and off-resonance frequency need to be simulated. A standard TrueFISP dictionary with the parameter ranges as shown in Table 1 leads to a total of 363,624 possible combinations and includes the parameter values that are commonly found in the human body. The computation of

Parameter	TrueFISP			FISP		
	Min value	Max value	Step size	Min value	Max value	Step size
T1 (ms)	100	2000	20	20	3000	10
	2000	5000	300	3000	5000	200
T2 (ms)	20	100	5	10	300	5
	100	200	10	300	500	50
	200	1900	200	500	900	200
Off-resonance (Hz)	-250	-190	20			
	-50	50	1			
	190	250	20			

Table 1: Ranges and step sizes used for the dictionary creation in case of a TrueFISP sequence (left) or FISP sequence (right).

such a dictionary for 1000 time points takes about 2.5 minutes on a standard desktop computer using a C++ based script and reaches 2.5 GB of memory size. A further increase in the dictionary size and/or resolution would increase the accuracy of the obtained maps at the expenses of an increase in the reconstruction time and memory requirements [19].

The simulation of a FISP acquisition is computed differently compared to the one described above. Since the FISP acquisition requires the simulation of multiple isochromats at different frequencies, which are then combined together, the simulation process through Bloch equations can be time consuming. An alternative time-efficient simulation is the extended phase graph (EPG) formalism [29], where a spin system affected by the sequence can be represented as discrete set of phase states, ideal to simulate the signal evolution of spins strongly dephased by unbalanced gradients. The FISP sequence is less sensitive to off-resonance effects compared to the TrueFISP acquisition, so the corresponding dictionary includes only the T1 and T2 relaxation times (Table 1) as the parameters of interest. This leads to 18,838 dictionary entries that can be computed in about 8 minutes on a standard desktop computer, and that generates a dictionary of about 1.2 GB.

Regardless of which sequence is used, the dictionary needs to be computed only once beforehand. It can then be used on the scanner, where it is used to reconstruct each MRF acquisition acquired with the sequence parameters that were simulated.

Matching

After the data acquisition, the fingerprint of each voxel (Fig. 2F) is normalized to unit norm and compared with all the normalized dictionary entries to identify the tissue in a given voxel (Fig. 2E). The simplest version of the matching is performed by taking the inner product between the voxel signal and each simulated fingerprint signal; the entry that returns the highest value is considered to be the one that best represents the tissue properties, and the respective T1, T2 and off-resonance values are assigned to the voxel (Fig. 2G). The relative spin density (M_0) map, instead, is computed as the scaling factor between the acquired and the simulated fingerprints. The inner product has been demonstrated to be a robust operation and is able to correctly classify the tissues even in case of low SNR due to undersampling or even in the presence of a limited amount of motion artifacts [19].

This approach has also the potential of distinguishing different tissue components present within a single voxel (partial volume effect) thanks

to the incoherence between different signal evolutions. The fingerprint (S) of a voxel containing different tissue can be seen as the weighted sum (w) of the different components (D): $S = Dw$. It has been shown [19] that, if the different components are known a priori, the appropriate inverse solution of the previous equation – $(D)^{-1}S = w$, where $(D)^{-1}$ represents the pseudoinverse of D – will provide the weight of each different tissue for each voxel [19,31].

The pattern recognition algorithm is performed on the scanner for every acquisition, so it is crucial for the clinical usefulness of the MR framework that this operation is performed in a reasonable time. While the direct matching using the inner product is accurate, it can take up to about 160 seconds to match a 2D slice of 128 x 128 base resolution, 1000 time points with a dictionary counting 363 624 entries. Similarly it takes about 30 seconds to match a 2D image with 256 x 256 voxels, 1000 time points and 18,838 dictionary entries for a FISP reconstruction.

The matching can be potentially accelerated by compressing the dictionary either in the time dimension or in the parameter combinations dimension, thus reducing the total number of comparisons that need to be performed. It has been shown [31] that the singular value decomposition (SVD) can be applied to compress the dictionary in the time dimension and reduce the matching time by a factor of 3.4 times for a TrueFISP dictionary and up to a factor of 4.8 times for a FISP dictionary. The SVD-based dictionary compression has less than 2% of reduction in the accuracy of the estimated parameters. In this approach, the dictionary is projected into a subspace of lower dimension spanned by the first 25-200 singular vectors obtained from the SVD. The acquired fingerprint is projected onto the same subspace, and the matching is performed using the projected signal and the compressed dictionary. This framework reduces the number of calculations, thus reducing the final computation time despite the added

operation of data projection on the subspace.

An alternative approach for reducing computational time for matching is by reducing the parameter combination dimension. A fast group matching algorithm [32] has been developed, where dictionary entries that have strong correlations are grouped together and a new signal that best represents the group is generated. The matching is thus subdivided in two steps; at first the acquired fingerprint is matched with the representing signal of each group, and only groups that return the highest correlation are kept in consideration. Then matching is used to find the best fit between the fingerprint and the remaining dictionary entries for the assignment of the parameters. This algorithm reduces the matching computation speed of one order of magnitude compared to the SVD compression and two orders of magnitude compared to the direct matching with no significant loss in the quality of the match. Techniques such as this make it feasible to implement MRF in a clinical manner.

Undersampling and motion

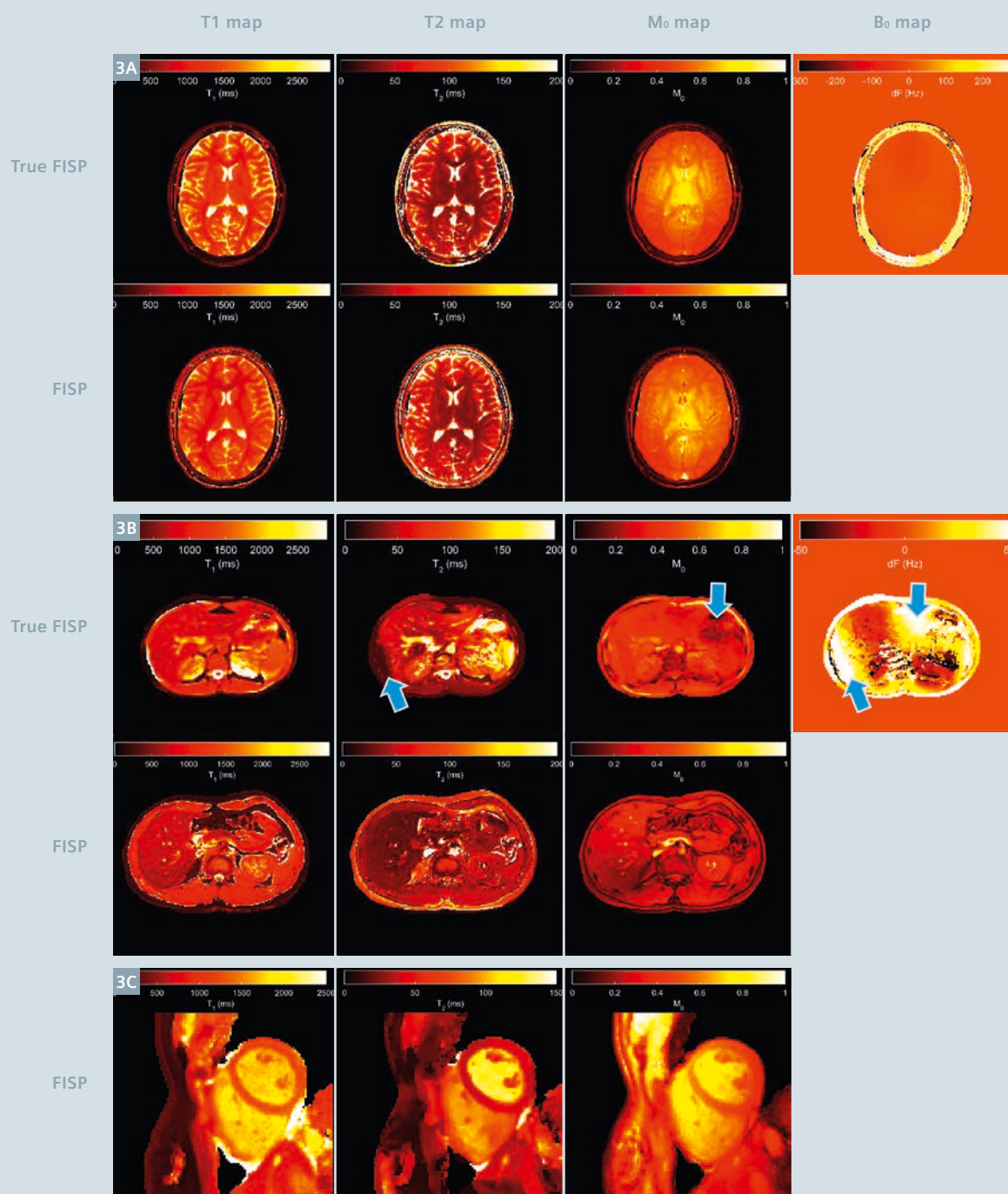
In MRF, the obtained parameter maps are the result of a pattern recognition algorithm as opposed to conventional reconstruction techniques, which allows MRF to be more robust to various image artifacts. This effect is strengthened by the random variation of FA, TR and trajectory which not only aim at differentiating the fingerprints from different tissues, but also aim at increasing the incoherence between the fingerprints. The matching can recognize the underlying signal evolutions even in low signal-to-noise or accelerated conditions as long as the noise or undersampling artifacts are incoherent with the signal. Additionally, just like in forensic fingerprinting, a correct identification is possible even with the use of blurry or partial fingerprints, the MR counterpart is also capable of providing parametric maps without any residual motion artifacts in case of a fingerprint partially corrupted by motion [19].

Volunteer acquisitions

MRF acquisitions have been tested in volunteers in 2D brain, abdominal, and cardiac scans. All *in vivo* experiments were performed under the Institutional Review Board guidelines and each subject signed informed consent prior to the data acquisition. The scans were performed on a 3T MAGNETOM Skyra system with a 20-channel head coil or a phased array 18-channel body coil plus spine coil. For the brain scans, the variable acquisition parameters (FA and TR) were set as described above and 3000 time points were acquired; the FOV was 300 x 300 mm, the slice thickness was 5 mm and the matrix size was 256 x 256. The acquisition time was 38 s for a 2D TrueFISP slice and 41 s for the FISP acquisition. The cardiac MRF scans were acquired using a modified pulse sequence with ECG triggering to restrict data collection to mid-diastole [35]. A total of 768 time points were acquired over a 16-heartbeats breath-hold using a scan window of 250 ms with FOV 300 x 300 mm, slice thickness 8 mm, and matrix size 192 x 192 [35]. For the abdominal and cardiac imaging, the trajectory and acquisition protocols were adapted as described in references [21, 35] respectively. The dictionaries were computed as described above and SVD based matching was used for parameter estimation.

Figure 3 shows the maps obtained from volunteer scans in the brain (Fig. 3A), abdomen (Fig. 3B), and heart (Fig. 3C). Both FISP and TrueFISP MRF provide comparable high resolution multiparametric tissue maps. The FISP acquisition has the drawback of not providing the off-resonance information, but it has the advantage of being insensitive to banding artifacts. Therefore, FISP MRF is advantageous for body imaging, where the sharp susceptibility transitions and the need for a large field-of-view would lead to banding artifacts with a balanced SSFP acquisition.

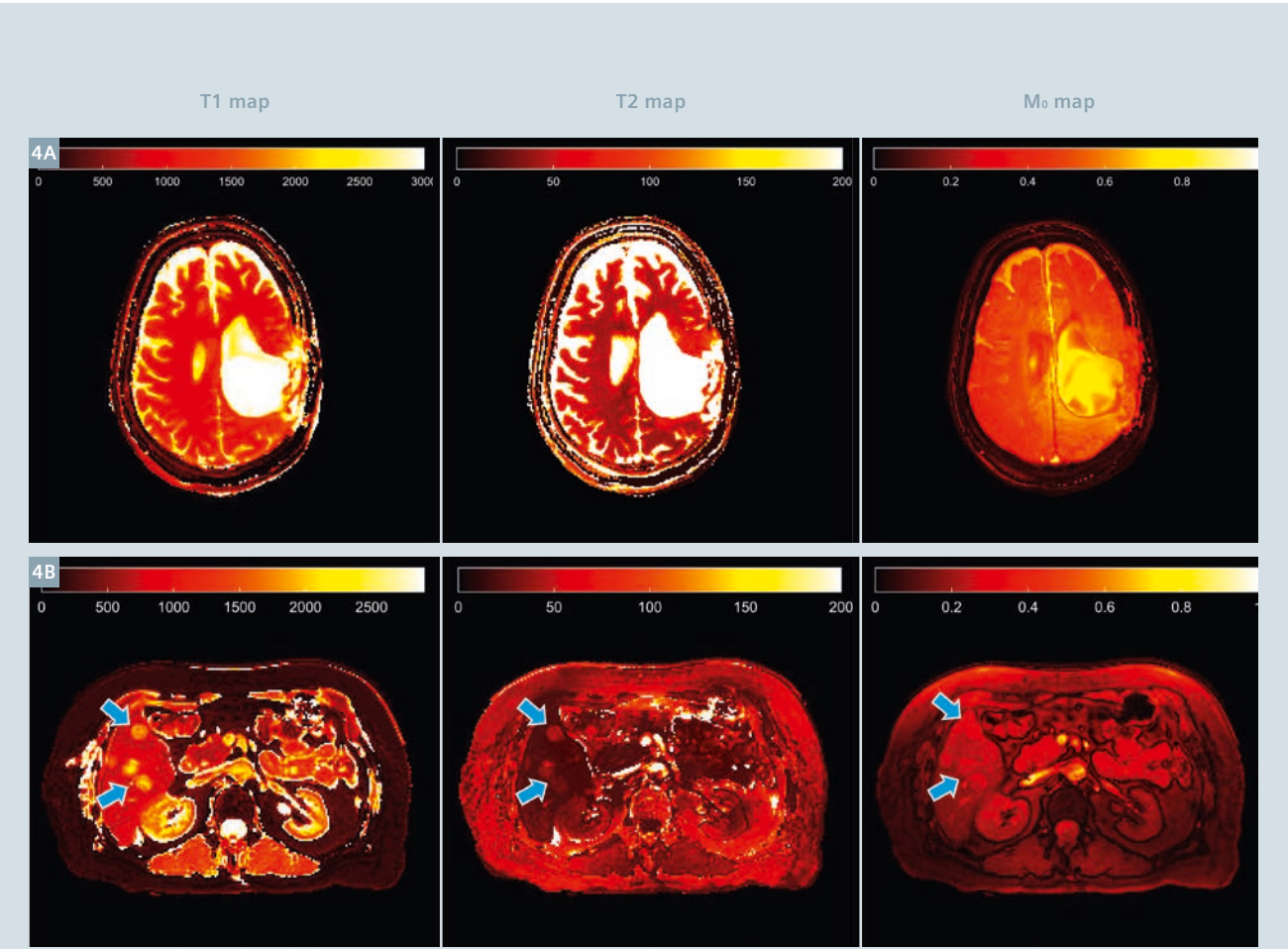
The values obtained with MRF maps are generally in good agreement with the standard mapping techniques [20] and with the literature value of tissue parameters [19, 24], as shown in table 2. It can be noticed, though,



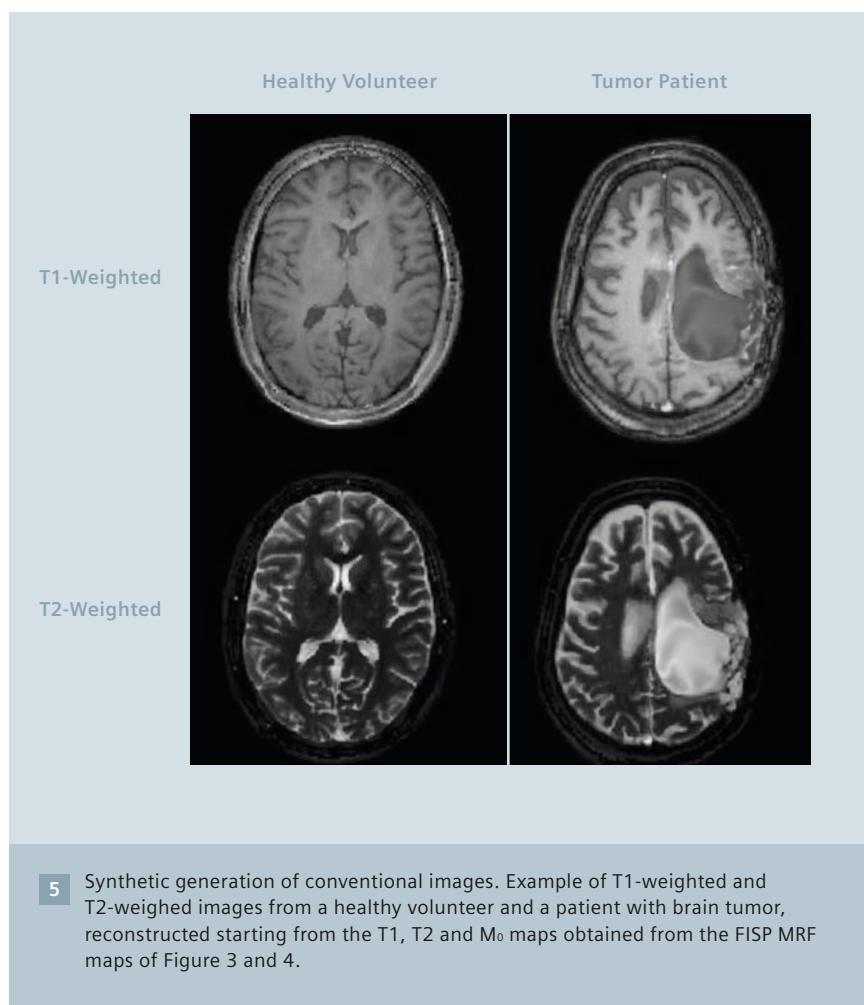
3 Examples of T1, T2, relative spin density (M_0) and off-resonance (B_0) maps acquired in two volunteers with a TrueFISP and a FISP acquisition. **(3A)** Single 2D slice of a head scan. **(3B)** Single 2D slice of an abdominal scan. **(3C)** Single 2D slice of diastolic cardiac scan in short axis view. In the T2 and B_0 map obtained from the TrueFISP acquisition, banding artifacts due to field inhomogeneity are visible (blue arrows).

Tissue	T1 (ms)		T2 (ms)	
	MRF	Literature	MRF	Literature
White matter	685 ± 33 [19]	608–756 [34, 40–42]	65 ± 4 [19]	54–81 [34, 40–42]
	781 ± 61 [20]	788–898 [43]	65 ± 6 [20]	78–80 [43]
Gray matter	1180 ± 104 [19]	998–1304 [34, 40–42]	97 ± 5.9 [19]	78–98 [34, 40–42]
	1193 ± 65 [20]	1286–1393 [43]	109 ± 11 [20]	99–117 [43]
Cerebrospinal fluid	4880 ± 379 [19]	4103–5400 [34, 40–42]	550 ± 251 [19]	1800–2460 [34, 40–42]
Liver	745 ± 65 [21]	809 ± 71 [44]	31 ± 6 [21]	34 ± 4 [44]
Kidney medulla	1702 ± 205 [21]	1545 ± 142 [44]	60 ± 21 [21]	81 ± 8 [44]
Kidney cortex	1314 ± 77 [21]	1142 ± 154 [44]	47 ± 10 [21]	76 ± 7 [44]
Skeletal muscle	1100 ± 59 [21]	1017 ± 78 [45]	44 ± 9 [21]	50 ± 4 [46]
Fat	253 ± 42 [21]	343 ± 37 [45]	77 ± 16 [21]	68 ± 4 [44]

Table 2: List of T1 and T2 relaxation times measured with MRF for different tissues and comparison with the value available in literature.



4 Example of patient results. Quantitative T1, T2 and relative spin density (M_0) maps obtained using the FISP protocol for brain [16] and abdomen acquisitions [20]. (4A) Maps of a patient with a brain tumor; (4B) 69-year-old patient with metastatic breast cancer. The metastasis (blue arrows) presents an increase in all tissue parameters, compared to the surrounding tissues.



that there is a mismatch in the values of CSF and fat. The CSF T2 discrepancy between MRF and literature value can be explained by through-plane motion of the fluid that was not taken into account in the dictionary simulation [19]. The fat T1 discrepancy, instead, is mainly due to the intentionally low T1 dictionary resolution (100 ms) for the range 100–600 ms used for that study [21].

The MRF efficiency is extremely high compared to traditional mapping approaches [19–21] as well as rapid combined T1 and T2 mapping methods like DESPOT [19, 36]. The high efficiency and accuracy of the MRF framework enable parametric mapping to be performed in a clinically relevant acquisition time without loss of information. In this way, multiparametric mapping can be translated to the clinical environment.

Patient acquisitions

The MRF framework has also been successfully tested on patients. Figure 4 shows the feasibility of brain and abdominal MRF in a clinical environment. Data were acquired with the previously described FISP acquisitions on patients with a brain tumor and breast cancer metastatic to the liver (Fig. 4). Longer T1 relaxation time can be observed in the metastatic lesions compared to the surrounding tissues. It has been shown in six patients with metastatic adenocarcinoma that the mean T1 and T2 values in the metastatic adenocarcinoma were on the order of 1673 ± 331 ms and 43 ± 13 ms, respectively. Those values are significantly higher than the ones of the surrounding tissues (840 ± 113 ms and 28 ± 3 ms, respectively) [21]. Recent studies investigate the possibility of predicting response of tumor

to treatment using tissue relaxation times; e.g. the T1 relaxation time can potentially be an indicator of chemotherapy response [35, 36]. Fast multiparametric mapping can thus open the path to the creation of a multiproperty space that might allow a deeper characterization and understanding of the conditions and evolutions of determined pathologies.

Synthetic weighted images

It is also possible to retrospectively calculate and estimate 'standard' weighted images from the multiple parameter maps obtained from an MRF scan. Figure 5 shows an example of T1-weighted and T2-weighted acquisition calculated from the FISP T1 and T2 maps of the volunteer and patient head scan shown above.

Conclusions

Magnetic resonance fingerprinting is a novel framework for MRI, where the pulse sequence design is not aimed at acquiring images, but at directly measuring tissue properties. In MRF, the sequence generates unique signal evolutions, or fingerprints, for each different tissue and matches it with a set of theoretical signal evolutions to measure several tissue properties within a single acquisition. Once the tissue features are measured, it is possible to directly know several tissue-specific properties that can synergistically provide all the information to improve diagnosis, prognosis and/or therapeutic assessment. In this work, only two MRF implementations have been shown, but the MRF framework has the potential to allow more freedom in the sequence design compared to standard MRI sequences, since the parameters can be randomly varied. Thanks to this freedom, a whole new world of possibilities of acquisition and reconstruction strategies that can probe and measure new features have been opened up for our community to explore.

This paper focused on T1, T2, M_0 and B_0 characterization, but the MRF is not limited to that. Several work are being performed to exploit the potential of MRF including: diffusion

[27], arterial spin labeling [28, 42, 43] and chemical exchange [44].

The pattern recognition nature of MRF makes the acquisition robust to artifacts like undersampling and motion, yielding high efficiency, accuracy and robustness that are critical for the successful integration of a multiparametric mapping technique into the clinical environment. Moreover, the increased efficiency and robustness to artifacts compared to standard MR imaging approaches could potentially reduce the time and thus the costs of MRI exams, making it more affordable and more competitive in comparison to other imaging modalities.

References

- Larsson H, Frederiksen J. Assessment of demyelination, edema, and gliosis by in vivo determination of T1 and T2 in the brain of patients with acute attack of multiple sclerosis. *Magn Reson Med* [Internet]. 1989;348:337–48. Available from: <http://onlinelibrary.wiley.com/doi/10.1002/mrm.1910110308/abstract>
- Usman AA, Taimen K, Wasielewski M, et al. Cardiac magnetic resonance T2 mapping in the monitoring and follow-up of acute cardiac transplant rejection: a pilot study. *Circ Cardiovasc Imaging* [Internet]. 2012;5(6):782–90. Available from: <http://www.ncbi.nlm.nih.gov/pubmed/23071145>
- Payne AR, Berry C, Kellman P, et al. Bright-blood T2-weighted MRI has high diagnostic accuracy for myocardial hemorrhage in myocardial infarction: a preclinical validation study in swine. *Circ Cardiovasc Imaging*. 2011;4(6):738–45.
- Van Heeswijk RB, Feliciano H, Bongard C, et al. Free-breathing 3 T magnetic resonance T2-mapping of the heart. *JACC Cardiovasc Imaging* [Internet]. 2012 Dec;5(12):1231–9. Available from: <http://www.ncbi.nlm.nih.gov/pubmed/23236973>
- Iles L, Pfluger H, Phrommintikul A, et al. Evaluation of Diffuse Myocardial Fibrosis in Heart Failure With Cardiac Magnetic Resonance Contrast-Enhanced T1 Mapping. *J Am Coll Cardiol*. 2008;52(19):1574–80.
- Hernando D, Levin YS, Sirlin CB, Reeder SB. Quantification of liver iron with MRI: state of the art and remaining challenges. *J Magn Reson Imaging* [Internet]. 2014 Nov;40(5):1003–21. Available from: <http://www.pubmed-central.nih.gov/articlerender.fcgi?artid=4308740&tool=pmcentrez&rendertype=abstract>
- Reeder SB, Cruite I, Hamilton G, Sirlin CB. Quantitative assessment of liver fat with magnetic resonance imaging and spectroscopy. *J Magn Reson Imaging* [Internet]. 2011 Oct;34(4):729–49. Available from: <http://www.ncbi.nlm.nih.gov/pubmed/21928307>
- Look DC, Locker DR. Time saving in measurement of NMR and EPR relaxation times. *Rev Sci Instrum*. 1970;41(2):250–1.
- Huang TY, Liu YJ, Stemmer A, Poncelet BP. T2 measurement of the human myocardium using a T2-prepared transient-state trueFISP sequence. *Magn Reson Med*. 2007;57:960–6.
- Mehta BB, Chen X, Bilchick KC, Salerno M, Epstein FH. Accelerated and navigator-gated look-locker imaging for cardiac T1 estimation (ANGIE): Development and application to T1 mapping of the right ventricle. *Magn Reson Med*. 2015;73(1):150–60.
- Zhu DC, Penn RD. Full-brain T1 mapping through inversion recovery fast spin echo imaging with time-efficient slice ordering. *Magn Reson Med*. 2005;54(3):725–31.
- Cheng H-LM, Wright GA. Rapid High-Resolution T1 Mapping by Variable Flip Angles: Accurate and Precise Measurements in the Presence of Radio-frequency Field Inhomogeneity. *Magn Reson Med*. 2006;55:566–76.
- Doneva M, Börner P, Eggers H, Stehning C, Sénégas J, Mertins A. Compressed sensing reconstruction for magnetic resonance parameter mapping. *Magn Reson Med*. 2010;64(4):1114–20.
- Deoni SCL, Rutt BK, Peters TM. Rapid combined T1 and T2 mapping using gradient recalled acquisition in the steady state. *Magn Reson Med*. 2003;49(3):515–26.
- Blume U, Lockie T, Stehning C, et al. Interleaved T1 and T2 relaxation time mapping for cardiac applications. *J Magn Reson Imaging*. 2009;29:480–7.
- Wartjes JBM, Dahlqvist O, Lundberg P. Novel method for rapid, simultaneous T1, T2*, and proton density quantification. *Magn Reson Med*. 2007;57(3):528–37.
- Schmitt P, Griswold MA, Jakob PM, et al. Inversion recovery TrueFISP: quantification of T(1), T(2), and spin density. *Magn Reson Med*. 2004;51(4):661–7.
- Ehses P, Seiberlich N, Ma D, et al. IR TrueFISP with a golden-ratio-based radial readout: Fast quantification of T1, T2, and proton density. *Magn Reson Med*. 2013;69(1):71–81.
- Ma D, Gulani V, Liu K, et al. Magnetic resonance fingerprinting. *Nature* [Internet]. 2013;495(7440):187–92.
- Jiang Y, Ma D, Seiberlich N, Gulani V, Griswold M a. MR fingerprinting using fast imaging with steady state precession (FISP) with spiral readout. *Magn Reson Med* [Internet]. 2014;. Available from: <http://www.ncbi.nlm.nih.gov/pubmed/25491018>
- Chen Y, Jiang Y, Pahva Shivani, et al. MR Fingerprinting for Rapid Quantitative Abdominal Imaging. *Radiology*. 2016;000(0):1–9.
- Schmitt P, Griswold MA, Gulani V, Haase A, Flentje M, Jakob PM. A simple geometrical description of the TrueFISP ideal transient and steady-state signal. *Magn Reson Med*. 2006;55(1):177–86.
- Perlin K. An image synthesizer. *ACM SIGGRAPH Comput Graph*. 1985;19(3):287–96.
- Ma D, Pierre EY, Jiang Y, et al. Music-based magnetic resonance fingerprinting to improve patient comfort during MRI examinations. *Magn Reson Med* [Internet]. 2015; Available from: <http://doi.wiley.com/10.1002/mrm.25818>
- Lee JH, Hargreaves B a., Hu BS, Nishimura DG. Fast 3D Imaging Using Variable-Density Spiral Trajectories with Applications to Limb Perfusion. *Magn Reson Med*. 2003;50(6):1276–85.
- Bloch F. Nuclear induction. *Phys Rev*. 1946;70:460–85.
- Jiang Y, Wright KL, Seiberlich N, Gulani V, Griswold MA. Simultaneous T1, T2, diffusion and proton density quantification with MR fingerprinting. In: In proceedings of the 22nd annual meeting of ISMRM meeting & exhibition in Milan, Italy. 2014. p. 28.
- Wright KL, Ma D, Jiang Y, Gulani V, Griswold MA, Luis H-G. Theoretical framework for MR fingerprinting with ASL: simultaneous quantification of CBF, transit time, and T1. In: In proceedings of the 22nd annual meeting of ISMRM meeting & exhibition in Milan, Italy. 2014. p. 417.
- Weigel M, Schwenk S, Kiselev VG, Scheffler K, Hennig J. Extended phase graphs with anisotropic diffusion. *J Magn Reson*. 2010;205(2):276–85.
- Deshmane AV, Ma D, Jiang Y, et al. Validation of Tissue Characterization in Mixed Voxels Using MR Fingerprinting. In: In proceedings of the 22nd annual meeting of ISMRM meeting & exhibition in Milan, Italy. 2014. p. 0094.
- McGivney D, Pierre E, Ma D, et al. SVD Compression for Magnetic Resonance Fingerprinting in the Time Domain. *IEEE Trans Med Imaging*. 2014;0062(12):1–13.
- Cauley SF, Setsompop K, Ma D, et al. Fast group matching for MR fingerprinting reconstruction. *Magn Reson Med* [Internet]. 2014;00. Available from: <http://dx.doi.org/10.1002/mrm.25439>
- Hamilton JI, Jiang Y, Chen Y, et al. MRF for Rapid Quantification of Myocardial T1, T2, and Proton Spin Density. *Magn Reson Med*. 2016;In press.

- 34 Deoni SCL, Peters TM, Rutt BK. High-resolution T1 and T2 mapping of the brain in a clinically acceptable time with DESPOT1 and DESPOT2. *Magn Reson Med*. 2005;53(1):237–41.
- 35 Jamin Y, Tucker ER, Poon ES, et al. Evaluation of Clinically Translatable MR Imaging Biomarkers of Therapeutic Response in the TH- MYCN Transgenic Mouse Model of Neuroblastoma. *Radiology*. 2012.
- 36 Weidensteiner C, Allegrini PR, Sticker-Jantscheff M, Romanet V, Ferretti S, McSheehy PM. Tumour T1 changes in vivo are highly predictive of response to chemotherapy and reflect the number of viable tumour cells - a preclinical MR study in mice. *BMC Cancer*. 2014;14(1):88.
- 37 Christen T, Pannetier NA, Ni WW, et al. MR vascular fingerprinting: A new approach to compute cerebral blood volume, mean vessel radius, and oxygenation maps in the human brain. *Neuroimage* [Internet]. 2014 Apr 1 [cited 2015 Nov 19];89:262–70. Available from: <http://www.pubmedcentral.nih.gov/articlerender.fcgi?artid=3940168&tool=pmcentrez&rendertype=abstract>
- 38 Pan S, Mao D, Peiying L, Yang L, Babu W, Hanzhang L. Arterial Spin Labeling without control/label pairing and post-labeling delay: an MR fingerprinting implementation. In: In proceedings of the 23rd annual meeting of ISMRM meeting & exhibition in Toronto, Canada. 2015. p. 0276.
- 39 Hamilton JI, Deshmane AV, Stephanie H, Griswold MA, Seiberlich N. Magnetic Resonance Fingerprinting with Chemical Exchange (MRF-X) for Quantification of Subvoxel T1, T2, Volume Fraction, and Exchange Rate. In: In proceedings of the 23rd annual meeting of ISMRM meeting & exhibition in Toronto, Canada. 2015. p. 0329.
- 40 Vymazal J, Righini A, Brooks RA, et al. T1 and T2 in the Brain of Healthy Subjects, Patients with Parkinson Disease, and Patients with Multiple System Atrophy: Relation to Iron Content. *Radiology*. 1999;211(2):489–95.
- 41 Whittall KP, MacKay AL, Graeb DA, Nugent RA, Li DK, Paty DW. In vivo measurement of T2 distributions and water contents in normal human brain. *Magn Reson Med*. 1997;37(1):34–43.
- 42 Poon CS, Henkelman RM. Practical T2 quantitation for clinical applications. *J Magn Reson Imaging*. 1992;2(5):541–53.
- 43 Wansapura JP, Holland SK, Dunn RS, Ball WS. NMR relaxation times in the human brain at 3.0 tesla. *J Magn Reson Imaging*. 1999;9(4):531–8.
- 44 de Bazelaire CM, Duhamel GD, Rofsky NM, Alsop DC. MR imaging relaxation times of abdominal and pelvic tissues measured in vivo at 3.0 T: preliminary results. *Radiology*. 2004;230(3):652–9.
- 45 Chen Y, Lee GR, Aandal G, et al. Rapid volumetric t1 mapping of the abdomen using three-dimensional through-time spiral GRAPPA. *Magnetic Resonance in Medicine*. 2016 Apr;75(4):1457–65.
- 46 Stanisz GJ, Odobina EE, Pun J, et al. T1, T2 relaxation and magnetization transfer in tissue at 3T. *Magn Reson Med* [Internet]. 2005/08/09 ed. 2005;54(3):507–12. Available from: <http://www.ncbi.nlm.nih.gov/pubmed/16086319>.

Contact

Vikas Gulani, M.D.
 Department of Radiology
 Case Western Reserve University
 University Hospitals Case Medical Center
 11100 Euclid Ave
 Bolwell Building, Room B120
 Cleveland, OH 44106
 USA
vxg46@case.edu

